

RSC Advances



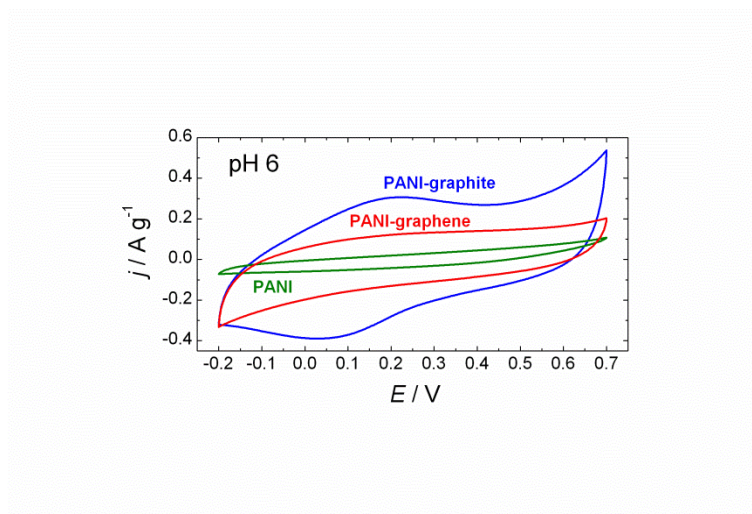
This is an *Accepted Manuscript*, which has been through the Royal Society of Chemistry peer review process and has been accepted for publication.

Accepted Manuscripts are published online shortly after acceptance, before technical editing, formatting and proof reading. Using this free service, authors can make their results available to the community, in citable form, before we publish the edited article. This *Accepted Manuscript* will be replaced by the edited, formatted and paginated article as soon as this is available.

You can find more information about *Accepted Manuscripts* in the [Information for Authors](#).

Please note that technical editing may introduce minor changes to the text and/or graphics, which may alter content. The journal's standard [Terms & Conditions](#) and the [Ethical guidelines](#) still apply. In no event shall the Royal Society of Chemistry be held responsible for any errors or omissions in this *Accepted Manuscript* or any consequences arising from the use of any information it contains.

Graphical abstract



The PANI-graphene/graphite composites show improved pH stability and electrochemical behaviour in aqueous electrolyte solutions at $\text{pH} \leq 8$ which can be utilized in solid-state chemical sensors and ion-selective electrodes.

Dispersible composites of exfoliated graphite and polyaniline with improved electrochemical behaviour for solid-state chemical sensor applications

Zhanna A. Boeva^{1,2,*}, Konstantin A. Milakin², Markus Pesonen³, Aleksander N. Ozerin⁴, Vladimir G. Sergeev² and Tom Lindfors^{1,*}

¹ Åbo Akademi University, Process Chemistry Centre, Department of Chemical Engineering, Laboratory of Analytical Chemistry, Biskopsgatan 8, FI-20500 Turku/Åbo, Finland

² M.V. Lomonosov Moscow State University, Chemistry Department, Polymer Division, Leninskie gory 1, build. 3, 119991 Moscow, Russian Federation

³ Åbo Akademi University, Department of Natural Sciences and Center for Functional Materials, Physics, Porthansgatan 3, FI-20500 Turku/Åbo, Finland

⁴ Russian Academy of Sciences, Institute of Synthetic Polymeric Materials, 70, Profsoyuznaya street, 117393 Moscow, Russian Federation

Abstract

We report here the *in situ* polymerization of aniline in the presence of exfoliated graphite of two different grades (graphene and graphite) resulting in composite materials which are readily dispersible in *N*-methylpyrrolidone. Compared to polyaniline (PANI) prepared without graphene/graphite which becomes electrically non-conducting already at pH > 3, the PANI-graphene/graphite composites showed significantly improved pH stability and electrochemical behaviour in aqueous electrolyte solutions at pH ≤ 8, without any further need of surface functionalization of the graphene/graphite flakes to stabilize the conducting form of polyaniline (PANI). The improved electroactivity is ascribed to the synergistic effect of graphene/graphite and PANI, and the network formation of the electrically conducting exfoliated graphites in the PANI matrix, which was electrochemically confirmed by simple cyclic voltammetric measurements at pH 9.5 in the presence of the Ru(NH₃)₆^{2+/3+} and Fe(CN)₆^{3-/4-} redox couples. Due to the dispersibility of the composites, thin films possessing stability in water can easily be prepared by solu-

* Corresponding authors: Tel: +74959393117, Fax: +74959390174. E-mail address: jbojeva@gmail.com (Zh.A. Boeva); Tel: +35822154419. E-mail address: Tom.Lindfors@abo.fi

tion casting for different types of solid-state chemical sensor and ion-selective electrode applications operating at neutral pH. By using sodium ascorbate as a model substance, we show that its amperometric detection at pH=7.3 with the PANI-graphite films results in a current amplification of 1.3-10.2 times in the concentration range of 10^{-4} - 10^{-2} M, compared to conventional PANI, which clearly demonstrates the advantage of incorporating exfoliated graphites in the PANI films. The materials reported in this paper were systematically characterized with cyclic voltammetry, FTIR, Raman and X-ray photoelectron spectroscopy, scanning electron microscopy, X-ray diffraction and electrical conductivity measurements.

1. Introduction

Graphene and graphene based composite materials have been extensively studied due to their outstanding electron mobility, mechanical strength and large specific surface area [1–3]. These properties make the use of graphene attractive in a wide range of applications ranging from sensors and actuators [4,5] catalytic layers [6], batteries [7,8], hydrogen storage materials to solar cells [9,10]. Apart from graphene, the intrinsically conducting polymers (ICPs) are efficient materials for various applications such as transparent antistatic coatings, nanoelectronics and chemical sensors [11-13]. Polyaniline (PANI) is one of the most studied ICP due to its excellent environmental stability, facile preparation, good electrical conductivity and the possibility to chemical modification [14]. The combination of ICPs with graphene, fullerenes and carbon nanotubes (CNTs) is greatly expected to promote the development of new materials with complementary properties and utilize the synergistic effect arising from non-electrostatic interactions of their conjugated structures [15,16].

Different methods have been recently proposed to prepare composites based on ICPs and graphene related materials. In most of these methods, the negatively charged and polar oxygen-containing surface groups (epoxy, hydroxyl, carbonyl and carboxyl) of graphene oxide (GO) function as charge compensating sites in the chemical or electrochemical polymerization of aniline, 3,4-

ethylenedioxythiophene or pyrrole [17–19]. Depending on the desired application, the ICP-GO composites can be deposited either as thin films on solid substrates, prepared as free standing powders or incorporated in conventional host polymeric materials, e.g. in hydrogels, for sensors applications [20–23]. It has been recently shown that thin composite films of poly(3,4-ethylenedioxythiophene) (PEDOT) and GO, and polypyrrole and GO were successfully synthesized by electrochemical polymerization from a GO solution without using additional dopants [24] and utilizing only the negative surface charge of GO. The electrically non-conducting GO in the ICP-GO composites can be further reduced [25–31] to remove most of the oxygen from its surface (resulting in the formation of reduced GO, rGO) to partially restore the sp^2 structure and electrical conductivity of graphene. The synergistic effect of PANI and rGO have been explored, for example, in PANI-rGO based supercapacitors having a high specific capacitance of $1046 \text{ F} \cdot \text{g}^{-1}$ in a three-electrode cell [32].

For a wider use of the PANI-graphene composites in many applications, it is crucial to improve their processability and dispersibility in common solvents. To solve this limitation, some successful solutions have been recently proposed to increase the dispersibility of the ICP-graphene composites. Bai et al. [33] have carried out non-covalent functionalization of GO with sulfonated PANI followed by reduction of GO to rGO. This approach results in a water dispersible sulfonated PANI-rGO composite with good electrochemical activity both at acidic and neutral pH. Another approach suggests the preparation of the dispersible PANI-graphene composites by first adsorbing aniline on the surface of the graphene platelets followed by polymerization of aniline [34]. Prepared in such a way, the composite material can be dissolved or dispersed in NMP but not in water, which is more beneficial for applications where the composite material becomes in contact with aqueous solutions.

It is well known that PANI usually loses its electrical conductivity at $\text{pH} \geq 3$ which limits its use in applications operating at the neutral or slightly alkaline pH (7.4) [35]. It is assumed that the incorpo-

ration of rGO or graphene into the PANI matrix can possibly solve this problem due to their electrostatic interactions preventing the deprotonation of PANI at neutral or slightly alkaline pH. As shown by Coskun et al., the composite films of PANI and sulfonated rGO retained their electroactivity still at $\text{pH} \leq 6$ in aqueous buffer solutions due to covalently attached sulfonic groups keeping the protons attached to the PANI backbone [36]. Recently, the electrochemical properties of the composite of rGO and PANI prepared with poly(4-styrenesulfonic) acid having different supermolecular structures were studied in the pH range of 1-9 [37, 38]. It was shown that due to the good pH stability of the composite, it retained its electroactivity in phosphate buffer solutions at $\text{pH} > 7$. Although their pH stability has not yet been reported, some of the composite materials of PANI and graphene derivatives have been used in chemical sensing applications for the detection of analytes such as H_2 , NH_3 , toluene, phenol, ascorbic acid, dopamine and uridine [39-43].

Despite that high-shear rate mixing of graphite was recently reported as a very promising method for industrial scale exfoliation of graphite to graphene [44], only thermally expanded graphites are currently commercially available as graphene nanoplatelets ranging from few-layered graphene to multi-layered graphite. Due to the simpler and more cost-effective preparation methods, the thermally exfoliated graphites are attractive materials in combination with ICPs. Moreover, the few- to multi-layered structure of the thermally exfoliated graphites may open the possibility of tuning the redox capacitance of the composite materials which could be beneficial in ion-to-electron transducers in solid-state ion-selective electrodes [45, 46] and in supercapacitor applications.

We have therefore used two different grades of exfoliated graphite to synthesize composite materials of PANI-graphene and PANI-graphite which are dispersible in NMP. These two grades have substantially different amount of graphene layers and surface area representing graphene and graphite produced by thermal expansion. Cyclic voltammetric measurements of thin composite films prepared on

glassy carbon substrates by drop-casting reveal that both graphene and graphite form an electrically conducting network in the PANI matrix. The PANI-graphene/graphite composite films which are stable in water (do not dissolve) showed improved pH stability for the conducting form of PANI and enhanced electrochemical activity at $\text{pH} \leq 8$, in comparison to neat PANI which lost its electroactivity at $\text{pH} > 3$. To the best of our knowledge, a systematic study of the influence of pH on the electroactivity of composite materials consisting of exfoliated graphites and PANI has not been previously reported. The improved electroactivity makes it possible to use the composite films as such, without pre-functionalization of graphene/graphite, in solid-state chemical sensor applications and as ion-to-electron transducers in solid-contact ion-selective electrodes operating at the neutral and slightly alkaline pH. We have used sodium ascorbate as a model substance to show that its amperometric detection with the PANI-graphite films at $\text{pH}=7.3$ gives significant signal amplification, especially at concentrations $\geq 10^{-3}$ M, due to the incorporation of graphite in the ICP matrix. The composite materials presented in this work have been characterized with cyclic voltammetry (CV), scanning electron microscopy (SEM), X-ray photoelectron spectroscopy (XPS), X-ray diffraction (XRD), Fourier transform infrared (FTIR) and Raman spectroscopy, and 4-point probe electrical conductivity measurements.

2. Experimental

2.1 Materials

Aniline (ANI) was received from Sigma-Aldrich and purified with distillation under reduced pressure. Exfoliated graphite of the AO-1 (< 3 monolayers of graphene) and AO-3 (graphite with 30-50 layered of graphene) grades were purchased from Graphene Supermarket. AO-1 and AO-3 have specific surface areas of $510 \text{ m}^2 \text{ g}^{-1}$ and $80 \text{ m}^2 \text{ g}^{-1}$, average flake thickness of 1.6 nm and 12 nm, and average

lateral sizes of ca. 10 μm and ca. 4.5 μm , respectively. Ammonium persulfate (APS, Sigma-Aldrich), ammonium hydroxide solution (25 wt%, p.a. grade, Emsure®, Merck), *N*-methylpyrrolidone (NMP, 99.5%, Riedel-de-Häen) and acetone (p.a. grade, J.T. Backer) were used as received. 1.0 M HCl and 1.0 M NaOH solutions were prepared using the Titrisol® titration standard solution (Merck). Hexaamineruthenium (II) chloride ($[\text{Ru}(\text{NH}_3)_6]\text{Cl}_2$), potassium hexacyanoferrate (II) ($\text{K}_4[\text{Fe}(\text{CN})_6]$) and sodium ascorbate were used as purchased from Sigma Aldrich. All the reagents were dissolved in deionized water (18.2 M Ω cm, ELGA PureLab Ultra system).

2.2 Aniline polymerization

The water solution of aniline (0.1 M) was mixed after sonication (30 min, 35 kHz, RF power 90 W) with 1.0 M APS dissolved in 1.0 M HCl resulting in a solution having the molar ratio of APS:ANI equal to 1. The reaction mixture was shortly shaken, ultrasonicated for 30 min and left to polymerize for 24 h at room temperature (RT). The resulting precipitate was first washed with deionized water and acetone until the washing liquid became colourless and then deprotonated with 10 wt% ammonium hydroxide overnight to convert PANI to the non-conducting emeraldine base (EB) form. The dry powder was then dissolved in NMP for 48 h under constant stirring and the obtained solution was centrifuged (Jouan, 5100 rpm, relative centrifugal force (RCF) ca. 3490). The soluble supernatant fraction was protonated with 1.0 M HCl solution and the precipitated electrically conducting emeraldine salt (ES) of PANI was washed with acetone to remove NMP residues which was monitored with FTIR spectroscopy until the vibrational band of the lactam stretching vibrations at 1680 cm^{-1} had disappeared from the spectrum. The purified precipitate was then dried in air for 24 h at room temperature (21 °C, RT).

2.3 PANI-exfoliated graphite composite preparation

A solution consisting of 0.1 M aniline and 0.2000 g exfoliated graphite (AO-1 or AO-3) was prepared by adding 91 μL of freshly distilled aniline (0.0930 g) to the exfoliated graphite followed by the addition of 10 mL deionized water. The obtained suspension was shortly shaken and then ultrasonicated for 30 min. The APS solution (1.0 M) dissolved in 1.0 M HCl (total volume: 1 mL) was thereafter added to the suspension, shortly shaken, ultrasonicated for 30 min and left to polymerize for 24 h at RT (similar to the aniline polymerization). Aniline, APS and HCl had all a final concentration of 0.091 M in the polymerization solution. The polymerization resulted in the precipitate containing either PANI(ES)-graphene (AO-1) or PANI(ES)-graphite (AO-3) and unreacted graphite, which was filtered, washed with water and acetone, and deprotonated to PANI(EB)-graphene and PANI/(EB)-graphite overnight with 10 wt% ammonium hydroxide solution. The deprotonated powder was then again filtered, washed with water and acetone, dried and then finally placed in NMP under constant stirring. After 48 h in NMP, the dispersion was centrifuged with the RCF of 3490 and what seemed to be an insoluble pristine (unreacted) graphite fraction was separated from the supernatant, washed with acetone and dried in atmospheric air. The supernatant containing either the PANI(EB)-graphene or the PANI(EB)-graphite composite was protonated and precipitated by adding 1.0 M HCl to the solution. The precipitates in the ES form were further washed with acetone to remove NMP residues as described above and dried in air for 24 h. Gravimetric analysis showed that the yield of the PANI(ES)-graphene and PANI(ES)-graphite composites were 18.5% and 5.1%, respectively, related to the theoretically calculated mass of PANI(ES) and exfoliated graphite used for the syntheses.

2.4 Composite characterization

The SEM measurements were performed using the LEO Gemini 1530 instrument (Oberkochen, Germany) equipped with a Thermo Scientific UltraDry Silicon Drift Detector (SDD, Thermo Scientific USA).

For the electrical conductivity measurements, the fully dispersible PANI, PANI-graphene and PANI-graphite powders were treated at pH 0 (in 1.0 M HCl) for 24 h and subsequently thoroughly washed with ethanol, dried, and pressed into pellets with 7.2 tons pressure at RT.

The conductivity of the samples was determined by 4-point probe measurements, in a linear configuration, having a tip spacing of 1.79 mm. The gold tips were spring-loaded to ensure good contact with the sample. A suitable bias current of 10^{-10} to 10^{-3} A was applied over the sample which depended on the sample resistance, and the corresponding voltage was measured with a Keithley 2400 SourceMeter®. The bias current was also provided by the same SourceMeter®. The conductivity of the samples was calculated using finite-size corrections [47]. All measurements were carried out in ambient conditions.

The XPS spectra were measured using the Phi Quantum 2000 instrument (Physical Electronics) with monochromatized Al K α as the radiation source. The XPS fittings were done with the PHI Multipak Version 9.0.0 software with the spectra calibrated against 284.8 eV. The bands were assigned based on available data in the literature and the NIST database [48].

The XRD spectra were collected using the Bruker D8 instrument with a focusing germanium crystal monochromator on a primary beam (CuK α_1 radiation, transmission mode). The scattering angle range 2θ was 10° – 100° and the powdered sample were placed between thin films of amorphous poly(ethylene terephthalate) and set onto a rotating platform in the instrument.

The Raman spectra were collected using the laser excitation wavelength of 514 nm (Renishaw; NIR diode laser) with the Renishaw Raman imaging microscope connected to the Leica DMLM microscope. Before the Raman measurements, the spectrometer was calibrated against the Si-standard (520.0 cm^{-1}).

The FTIR spectra were carried out in the transmission mode using the Bruker IFS 66/S instru-

ment with the accumulation of 128 interferograms per spectrum with the resolution of 4 cm^{-1} . All samples were mixed with KBr and pressed into pellets with 7.2 tons pressure.

All electrochemical characterizations of the composite films were done with CV in a three-electrode cell with the scan rate of 50 mV s^{-1} . The glassy carbon (GC) disc electrode encapsulated in a polyether ether ketone (PEEK) body served as the working electrode (WE) and the PANI-graphene or PANI-graphite film was drop-casted ($10\text{ }\mu\text{L}$) on the GC surface. A GC rod and Ag/AgCl/3M KCl electrode was used as counter and reference electrodes, respectively. The redox measurements were carried out in an aqueous solutions of $1\text{ mM [Ru(NH}_2)_6\text{]Cl}_2$ or $\text{K}_4\text{[Fe(CN)}_6\text{]}$ in 0.1 M KNO_3 as the background electrolyte (BGE) under inert nitrogen gas atmosphere. The electrochemical activity of the composite materials at different pH values was also determined under inert nitrogen atmosphere in NaCl/HCl/NaOH solutions by using the SnO_2 -glass coated with a thin layer (10 nm) of sputtered Pt as the WE. The pH was adjusted to the desired value by adding HCl or NaOH to the NaCl solution by maintaining the ionic strength at 0.1 M ; except for pH 0 where the ionic strength was 1 M . The voltammetric detection of ascorbate was carried out only with the neat PANI and PANI-graphite composite in 0.1 M KNO_3 as the BGE.

3. Results and Discussion

3.1. Characterization of the graphene and graphite starting materials

The SEM images of the graphene and graphite starting materials are shown in Fig. 1. The images reveal that due to their multilayered structure, the graphite flakes (Fig. 1b) are slightly more flat and robust than the graphene flakes (Fig. 1a). It should be noted that both flake types have a relatively high size distribution which can affect the dispersibility of the PANI-graphene and PANI-graphite composites

in NMP, as well as the surface morphology of the drop-casted composite films. One can therefore expect that the smaller flakes of the carbon material will be easier incorporated in the composite materials. This is due to the better colloidal stability of the smaller particles of graphene and graphite, and their higher reactivity with PANI compared to the larger flakes which is most likely caused by the higher density of edge groups. In Fig. 2, the different XRD patterns clearly demonstrate the differences in the graphene (AO-1) and graphite (AO-3) materials. The graphite powder has a sharp (002) diffraction peak at 26.6° corresponding to the interlayer distance of 0.344 nm which is close to natural graphite (0.335 nm) [49]. On the other hand, the graphene powder has two (002) peaks at 25.6° and 16.4° related to 0.355 and 0.545 nm, respectively. The former interlayer distance of the few-layered graphene is somewhat larger compared to natural graphite while the latter (0.545 nm) is significantly higher and usually observed in GO which has the diffraction peak at 14.85° [50]. This peak corresponds to defects in the graphene structure induced by covalently attached hydrophilic oxygen-containing groups on its surface [50]. Moreover, the total intensity of the XRD diffractogram of graphene is significantly lower compared to the XRD pattern of graphite which is typical for few-layered graphene [51].

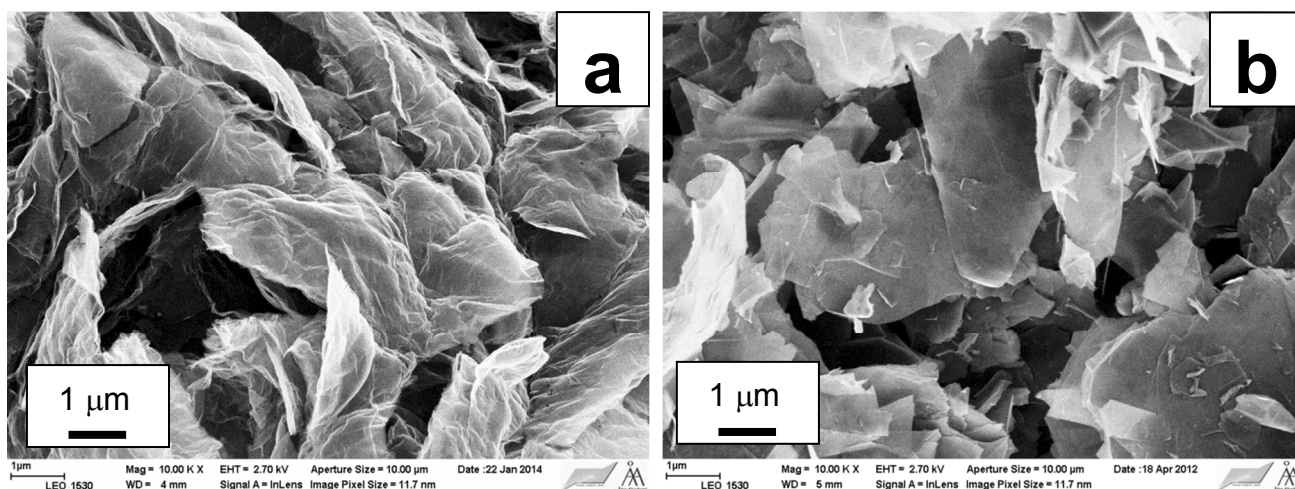


Fig. 1. SEM images of (a) graphene (< 3 monolayers; average flake thickness: 1.6 nm; average lateral

particle size: $\sim 4.5 \mu\text{m}$) and **(b)** exfoliated graphite (30-50 monolayers; 12 nm; $\sim 10 \mu\text{m}$). Magnification: 10000 x.

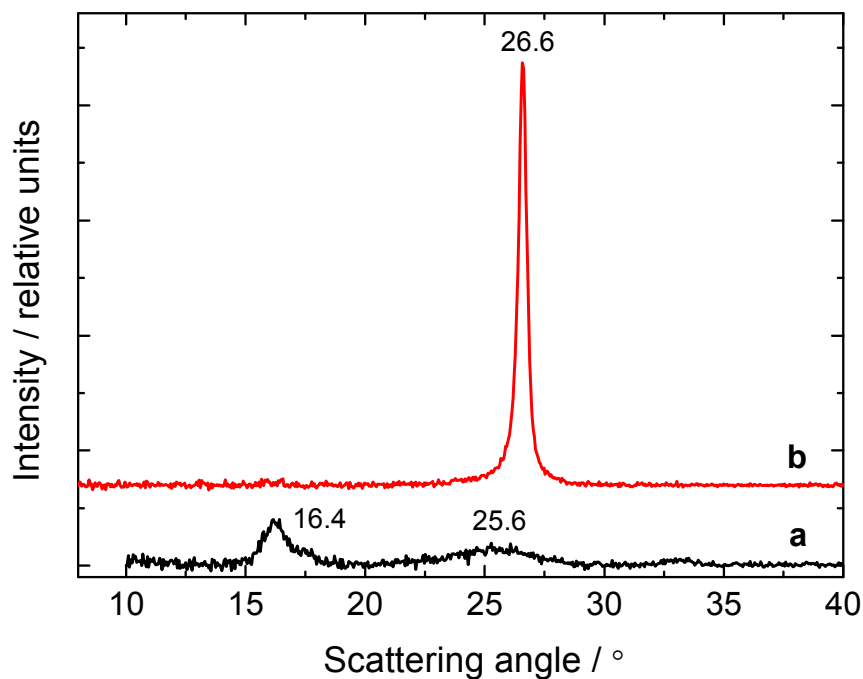


Fig. 2. XRD pattern of **(a)** graphene (< 3 monolayers) and **(b)** exfoliated graphite (30-50 monolayers).

In the chemical synthesis of the composite materials, the interaction of PANI with graphene or graphite can occur via π - π -stacking of the benzene rings of PANI and the condensed rings of graphene. Other possible ways are electrostatic interactions or hydrogen bonding between nitrogen atoms of PANI and the oxygen-containing surface groups originating from the preparation procedure of the exfoliated graphites. Therefore, XPS analysis was carried out on the few-layered graphene and graphite to evaluate their chemical surface composition (Fig. 3).

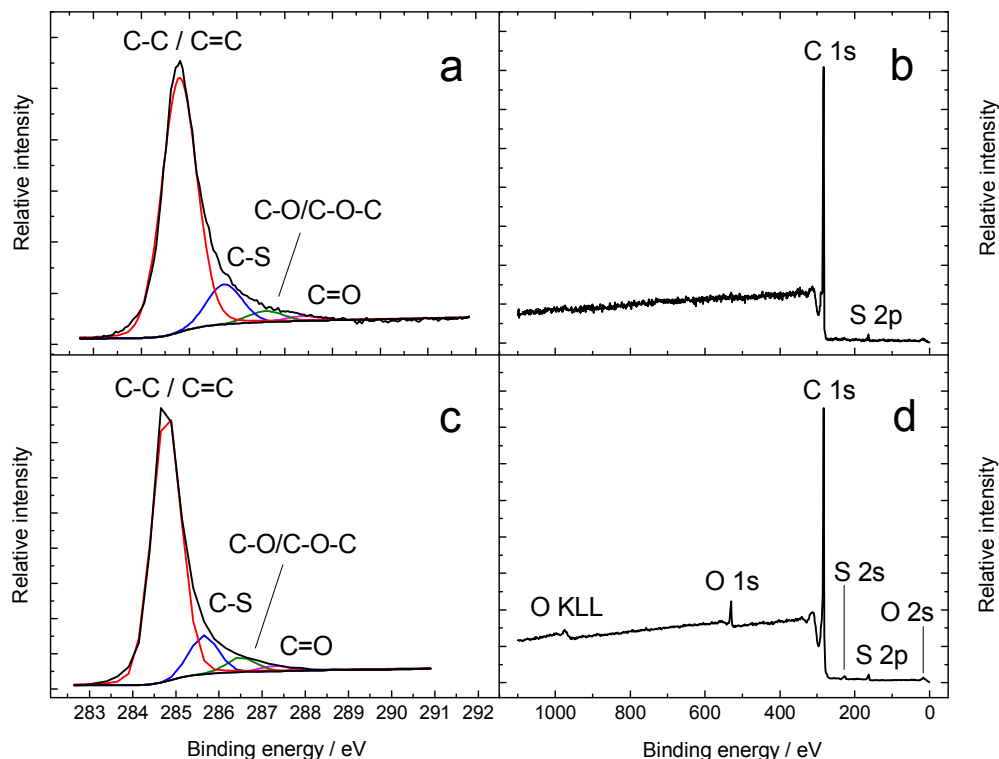


Fig. 3. The XPS spectra of **(a, b)** graphene (< 3 monolayers) and **(c, d)** exfoliated graphite (30-50 monolayers). Figures (a) and (c) show the C 1s spectra with $\chi^2=7.1$ and $\chi^2=64.4$, respectively.

In Fig. 3b and 3d, the XPS spectra of the full binding energy range show that graphite contains substantially more oxygen (3.2%) and sulphur (0.9%) than the few-layered graphene (O: 0.8%; S: below the detection limit). The elemental composition gives approximate C:O ratios of 30 and 127.5 for graphite and few-layered graphene, respectively, revealing that graphene has lower amounts of surface functional groups and defects than graphite. The C 1s spectra of graphene and graphite were fitted to four different bands (Fig. 3a and 3c). For both carbon materials, the intensive peak at 284.8 eV originating from the C-C/C=C bonds of the carbon lattice (sp^3/sp^2 hybridization) is accompanied with the less intensive peaks at 285.7, 286.5 and 287.3 eV which are assigned to the C-S, C-O/C-O-C (epoxy and hydroxyl)

and C=O groups, respectively. Therefore, the minor amounts of oxygen and sulphur originating from the exfoliation process may to some extent be capable to interact with PANI during the synthesis of the composite materials and therefore facilitate the formation of PANI on the graphene/graphite surface.

The vibrational analysis of graphene and graphite shows that their FTIR spectra are featureless due to the symmetry constrains of the method (Fig. S1). However, the Raman spectra of both materials slightly differ from each other (Fig. S2 and Table S1). The spectrum of graphite contains D and G bands at 1347 and 1570 cm^{-1} (D/G band intensity ratio: 0.74), respectively, corresponding to defect zones and the degenerated E_{2g} mode. In the Raman spectrum of graphene, the D and G bands at 1344 and 1579 cm^{-1} having the D/G intensity ratio of 1.27 shows that there is more disorder in the few-layered graphene compared to graphite.

3.2. PANI-graphene and PANI-graphite composite materials

As shown in the Fig. 4a, the chemical synthesis of PANI at pH 1 with APS as the oxidizing agent and HCl as the dopant results in the formation a polymer with granular morphology [52]. The polymerization under the same synthesis conditions in the presence of graphite gave a mixed morphology with the graphite flakes surrounded by granular PANI particles (Fig. 4b). The influence of the exfoliated graphites on the surface morphology was even more pronounced when the synthesis was performed with the few-layered graphene revealing a densely packed structure in which neither the typical PANI grains nor graphene flakes could be distinguished (Fig. 4c).

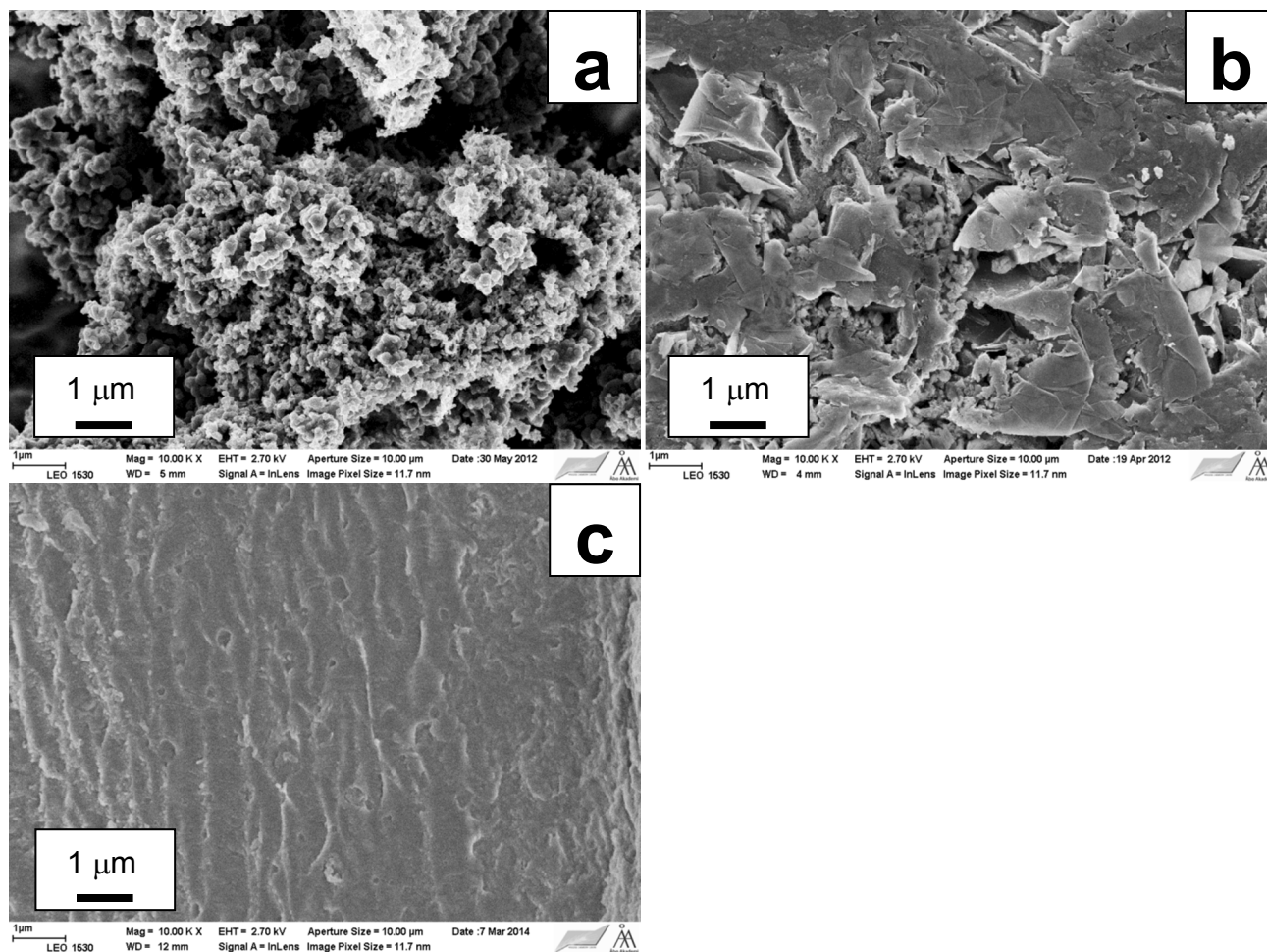


Fig. 4. SEM images of (a) PANI(ES)-Cl and the (b) PANI(ES)-graphite and (c) PANI(ES)-graphene composites. Magnification: 10000x

As shown in Fig. S1c-e, the FTIR spectra of the neat PANI(ES), PANI(ES)-graphene and PANI(ES)-graphite composites have absorption bands at 1556/1556/1558 and 1479/1479/1483 cm^{-1} assigned to the quinoid (Q) and benzoid (B) rings of PANI, respectively, confirming the presence of PANI in the composite materials [53,54]. This is further verified by the N 1s band in the XPS spectra of the composite materials (not shown) and by the vibrational bands of PANI(ES)/PANI(ES)-graphene/PANI(ES)-graphite at 1119/1113/1144 cm^{-1} , 1236/1236/1242 cm^{-1} and 1292/1290/1300 cm^{-1} in the FTIR spectra which are assigned to the $\text{C}_{\text{ar}}\text{-N}$ stretching vibrations, protonated imine nitrogen bonds

and in-plane C-H vibrations of the N=Q=N, Q=N⁺H-B, B-N⁺H-B groups [54]. In Figs S1d and S1e, the broadening of the C_{ar}-N stretching band at ca. 970 cm⁻¹ (shoulder) may originate from the incorporation of graphene and graphite in the PANI(ES) matrix. In comparison to the vibrational bands of PANI(ES)-graphene, the PANI(ES)-graphite bands show clear shifts compared to the PANI(ES) bands indicating that exfoliated graphite interacts stronger with PANI than the few-layered graphene. This is in good accordance with the results of the CV measurements presented below. Moreover, the higher amount of oxygen-containing surface groups of graphite results probably in more efficient interaction with PANI(ES) due to hydrogen bonding.

The Raman spectra and the vibrational bands of the PANI-graphite/graphene composite are shown in Fig. S2 and summarized in Table S1. In the PANI(EB) spectrum in Fig. S2 (spectrum c), the stretching vibrations of the Q rings at ~1557-1562 cm⁻¹ and the C-N⁺ stretching vibrations of the semiquinone radicals in the aryl rings at ~1340-1352 cm⁻¹ (which are usually present also in the spectrum of the EB form) strongly overlap with the D and G bands of graphene and graphite (spectra a and b). Hence, it is not possible to distinguish the D and G bands of graphene/graphite in PANI(EB)-graphene and PANI(EB)-graphite composites (spectra d and e) due to the vibrationally enhanced PANI(EB) bands. Possibly the slight broadening of the semiquinone radical band of the PANI(EB)-graphene composite at ~1340-1352 cm⁻¹ can be attributed to the presence of graphene. It has been previously observed for composite materials of PEDOT-GO that the vibrationally enhanced PEDOT bands have much higher intensities than GO. This shows that Raman spectroscopy is not the most suitable tool for verifying the incorporation of graphene/graphite and its derivatives in composite materials with ICPs [24,55].

It was recently shown that the formation of an electrically conducting network of rGO in the poly(*N*-methylaniline) (PNMA) matrix could be verified by CV measurements with the Ru(NH₃)^{2+/3+} redox couple [56]. In the potential interval where PNMA is electrically non-conducting (-0.6 to 0.15 V

vs. Ag/AgCl/3 M KCl), the incorporation of the conducting rGO in the PNMA matrix still provided electron transfer pathways within the PNMA-rGO material and therefore made it possible to detect the redox reaction of the $\text{Ru}(\text{NH}_3)^{2+/3+}$ couple in aqueous solution. Hence, to prove the incorporation of graphene or graphite in the PANI matrix, we have performed similar CV measurements in aqueous solutions of 1 mM $[\text{Ru}(\text{NH}_3)_6]\text{Cl}_2$ (Ru(II); pH=9.5), but also in 1 mM $\text{K}_4\text{Fe}(\text{CN})_6$ (Fe(II); pH=7.8), by cycling the potential between -0.6-0.15 V and -0.2-0.7 V, respectively (Fig. 5). At these pH values, the UV-vis spectra of the composite films measured at equilibrium show the characteristic feature of PANI in the non-conducting EB form [57]. (Fig. S3). Moreover, the polymer matrix should be in the electrochemically inactive leucoemeraldine (LE) base form in the potential range of -0.6 – 0.15 V (*cf.* with the CV of PANI in Fig. 6a, curve 1). Therefore, any electrochemical response of the PANI-graphene and PANI-graphite composites can only originate from electron transfer through the conducting pathways of graphene/graphite in the PANI matrix. In the redox measurements, the currents observed in the CVs are proportional to the extent of the oxidation and reduction reactions of the $\text{Ru}(\text{NH}_3)^{2+/3+}$ and $\text{Fe}(\text{CN})_6^{3-/4-}$ redox couples occurring at the composite film surface.

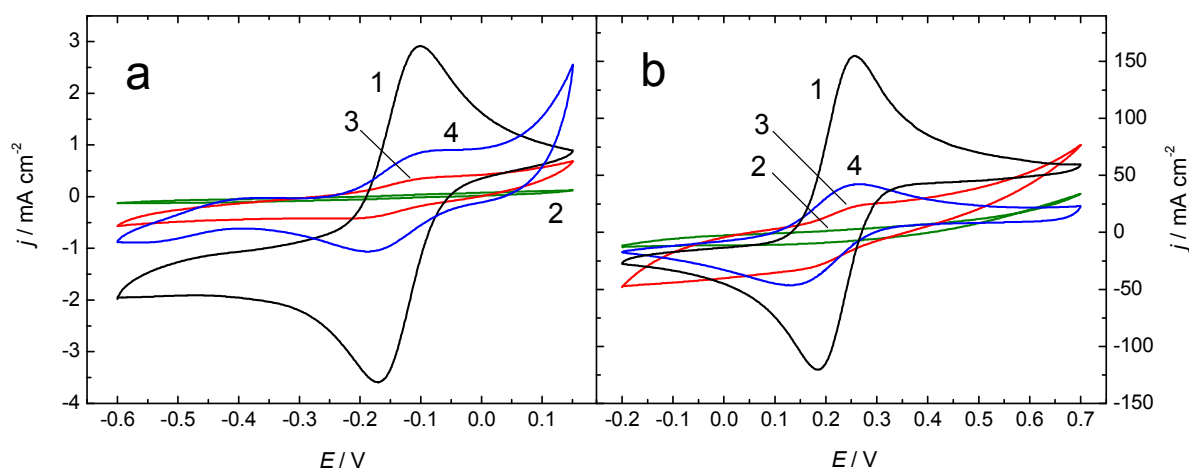


Fig. 5. Cyclic voltammograms of (1) the glassy carbon substrate, (2) neat PANI, (3) PANI-graphene and

(4) PANI-graphite films measured in an aqueous solution of **(a)** 10^{-3} M $[\text{Ru}(\text{NH}_3)_6]\text{Cl}_2$ (pH=9.5; 5th cycle shown) and **(b)** 10^{-3} M $\text{K}_4[\text{Fe}(\text{CN})_6]$ (pH=7.8; 3rd cycle). Background electrolyte: 0.1 M KNO_3 ; $v=50$ mV s^{-1} ; Reference electrode: $\text{Ag}/\text{AgCl}/3$ M KCl .

The curve 1 in Figs 5a and 5b shows the CVs recorded in 1 mM $[\text{Ru}(\text{NH}_3)_6]\text{Cl}_2$ and 1 mM $\text{K}_4\text{Fe}(\text{CN})_6$ on bare GC, which was used as the electrode substrate for the PANI, PANI-graphene and PANI-graphite films. In both cases, the redox processes were almost reversible showing close to theoretical oxidation and reduction peak potential differences (ΔE_p) of 0.068 V and 0.072 V for the $\text{Ru}(\text{NH}_3)_6^{2+/3+}$ and $\text{Fe}(\text{CN})_6^{3-/4-}$ redox couples, respectively. On GC, the ruthenium redox couple had the oxidation/reduction peak potentials ($E_{p,\text{ox}}/E_{p,\text{red}}$) at -0.101 V/-0.169 V while for the iron couple, the redox reaction occurred at the positive potentials of 0.256 V/0.184 V. As shown by curve 2 in Figs 5a and 5b, the PANI films deposited on GC do not show any noticeable electrochemical activity in the studied potential intervals due to their electrically insulating nature at alkaline pH (7.8 and 9.5). In contrast to the PANI film, the CVs of the PANI-graphene (curves 3) and PANI-graphite (curves 4) composites reveal distinct electrochemical activity for both redox couples. For the ruthenium redox couple, the PANI-graphite film shows the highest electroactivity and current density of these two materials ($\Delta E_p = 0.079$ V; $E_{p,\text{ox}}/E_{p,\text{red}} = -0.103$ V/-0.182 V) indicating that graphite forms a network with a higher conductivity in the PANI matrix compared to graphene. For the PANI-graphene, the current density is therefore lower than for PANI-graphite although the peak separation of 0.084 V is almost the same ($E_{p,\text{ox}}/E_{p,\text{red}} = -0.093$ V/-0.177 V). The peak separation potentials of PANI-graphene and PANI-graphite are just slightly higher than for GC which confirms the good reversibility of the ruthenium redox process for both composite materials. The current densities of the electrodes modified with PANI-graphene and PANI-graphite are lower compared to the bare GC electrode. The reason for this is the lower electrical conductivity of the composite materials at the alkaline pH compared to GC. In the composites, the graphene and graphite

platelets are presumably partially covered and surrounded with PANI. As PANI is deprotonated at pH=7.8 and 9.5, and thus does not participate in the electron transfer (Fig. 5, curves 2), the lower current densities observed in the presence of the redox couple are therefore caused by the slower charge transfer in the composite matrices (e.g. due to tunneling effects). Additionally, it is reasonable to assume that because of the inactivity of PANI, the graphene/graphite in the composite material has a smaller available active surface area for the electrochemical reaction to occur compared the GC surface contributing to the lower current density.

The redox measurements of the composite materials in the presence of the $\text{Fe}(\text{CN})_6^{3-/4-}$ redox couples show the same reversible behaviour as was observed with the ruthenium couple. As Fig. 5b reveals, the PANI-graphite composite ($\Delta E_p=0.131$ V; $E_{p,ox}/E_{p,red}= 0.265$ V/0.134 V) has slightly higher electrochemical activity than PANI -graphene ($\Delta E_p=0.085$ V; $E_{p,ox}/E_{p,red}= \text{ca. } 0.265$ V/ca. 0.165 V). This is in good accordance with the four-probe electrical conductivity measurements revealing that PANI(ES)-graphite (2.97 S cm^{-1}) had ca. 8 times higher electrical conductivity than PANI(ES)-graphene (0.37 S cm^{-1}). The higher electrical conductivity and electroactivity of PANI-graphite is most likely due to the ca. 9 times higher electrical conductivity of the exfoliated graphite (532 S cm^{-1}) compared to the few-layered graphene (57 S cm^{-1}). However, the electrical conductivities were measured on pellets pressed of PANI-graphene and PANI-graphite powders and because of the possible differences in their bulk and surface morphology, the obtained conductivity values may not be in full accordance with the electrochemical redox responses of the drop-casted composite films measured in the presence of the $\text{Ru}(\text{NH}_3)_6^{2+/3+}$ and $\text{Fe}(\text{CN})_6^{3-/4-}$ redox couples.

We have also investigated how the incorporation of graphene and graphite in the PANI matrix influenced the electrochemical activity of the composite materials in the pH interval of 0-10, due to the possible applications of the PANI-graphene/graphite in solid-state chemical sensors operating at neutral

or slightly alkaline pH. For this purpose, thin films of the composite materials and the neat PANI was prepared by drop castings on electrically conducting Pt/SnO₂ glass substrates and their electrochemical properties were studied with CV at different pH (Fig. 6).

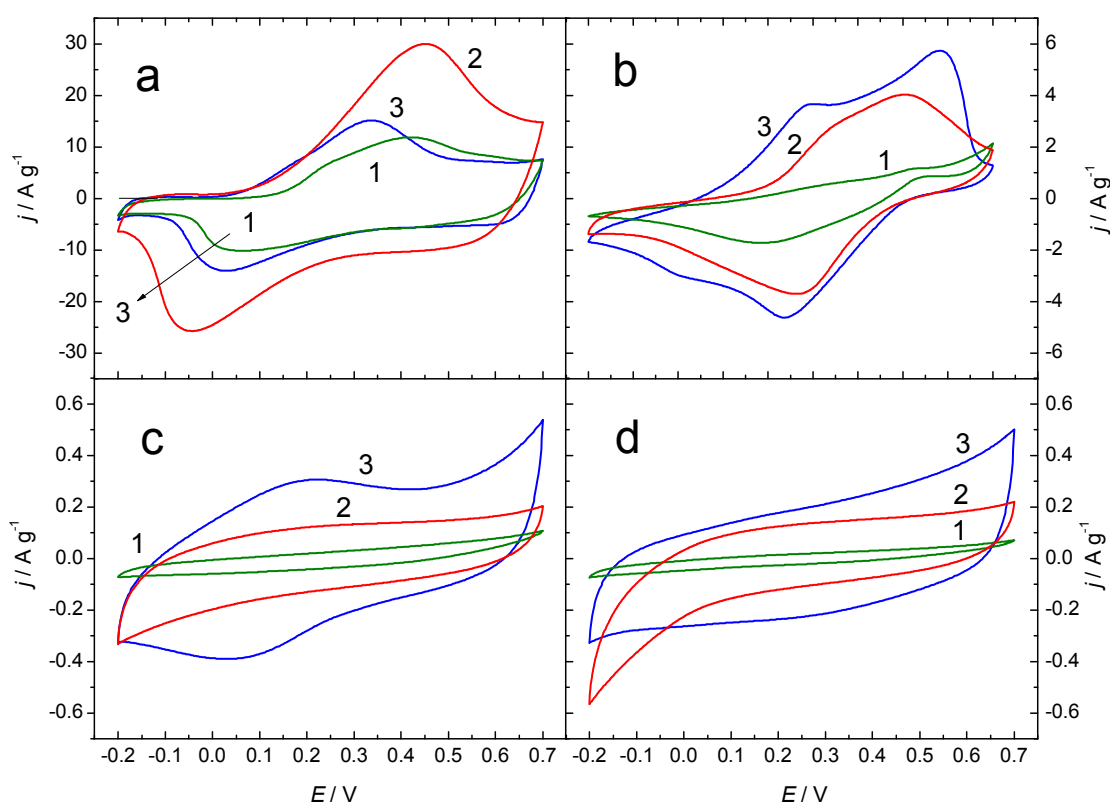


Fig. 6. Cyclic voltammograms (1) neat PANI, (2) PANI-graphene and (3) PANI-graphite films measured at (a) pH=0, (b) pH=3, (c) pH=6 and (d) pH=8. Supporting electrolyte: 0.1 M NaCl at pH 3, 6 and 8. pH was adjusted either with HCl or NaOH. Reference electrode: Ag/AgCl/3 M KCl; $v=50 \text{ mV s}^{-1}$.

In 1.0 M HCl at pH 0 (Fig. 6a), the CVs reveal that the PANI-graphene composite showed the highest gravimetric current density (30.0 A g^{-1} at $E_{p,ox}=0.452 \text{ V}$; $\Delta E_p=0.456 \text{ V}$) followed by PANI-graphite (15.1 A g^{-1} at $E_{p,ox}=0.338 \text{ V}$; $\Delta E_p=0.309 \text{ V}$) and neat PANI (11.8 A g^{-1} at $E_{p,ox}=0.417 \text{ V}$; $\Delta E_p=0.349 \text{ V}$). Thus, the CVs in Fig. 6a clearly demonstrate the advantage of incorporating the few-layered

graphene and exfoliated graphite in the ICP matrix. It should be stressed that the reason for the higher electroactivity of the PANI-graphene film compared to PANI-graphite at pH 0 is still unclear. However, although the bulk electrical conductivity of PANI-graphene (0.37 S cm^{-1}) was lower than for PANI-graphite (2.97 S cm^{-1}) and neat PANI (1.35 S cm^{-1}), it must be kept in mind that in the CV measurements, the films are perturbed from their equilibrium state and forced to be oxidized and reduced (LE-ES transition) during the potential cycling. They can therefore be brought to a higher protonation level (*i.e.* higher electrical conductivity) during the CV measurements compared to protonation at equilibrium (open circuit conditions), which was used to protonate the pressed pellets for the electrical conductivity measurements. The potential cycling may also cause morphological changes in the film which can influence their oxidation and reduction behaviour.

When the CVs were recorded at pH 3, the neat PANI film lost to a great extent its electrochemical activity with the gravimetric current density diminishing in magnitude which is in good accordance with previous reports in the literature (Fig. 6b) [58]. The CV of PANI shows only one bigger reduction peak at 0.18 V caused by the ES to LE conversion, in contrast to both PANI-graphene and PANI-graphite showing much higher electrochemical activity. Two reversible oxidation and reduction peaks corresponding to the LE/ES and the ES/permigraniline transitions in PANI can be seen in the CVs of PANI-graphene and PANI-graphite [59]. The CVs clearly reveal that both composite materials retain their electroactivity to a considerably higher extent than neat PANI at pH=3. Fig. 6b shows that the PANI-graphite composite is oxidized to the electrically conducting ES form already at *ca.* 0.05 V, which is *ca.* 0.1 V lower than for PANI-graphene, indicating that the exfoliated graphite possesses a higher electroactivity than the few-layered graphene. This can also be explained with the higher amount of the oxygen-containing groups on the surface of the exfoliated graphite sheets compared to the few-layered graphene sheets (see 3.1 XPS measurements). The carboxyl and hydroxyl groups can interact with PANI

via electrostatic forces and hydrogen bonding and thus, in analogy with bulky counterions increase the stability of the ES form and retain the electrochemical activity at higher pH [35, 60].

At pH 6, the CVs of PANI-graphite show still much higher electroactivity than PANI-graphene and PANI (Fig. 6c). Especially PANI has almost entirely lost its electroactivity and no faradic currents are therefore observed due to deprotonation of PANI, while the CV of PANI-graphite has clearly distinguishable oxidation and reduction peaks at 0.222 V and 0.032 V, respectively. It should be noted that the gravimetric current density is 0.3 A g^{-1} at the oxidation peak potential of PANI-graphite which is only ca. 2% of its value at pH 0 (15.1 A g^{-1} at $E_{p,ox}=0.337 \text{ V}$). However, despite of the much reduced electroactivity of both PANI-graphene and PANI-graphite at pH 6, their electroactivity should be still high enough to carry out the electrochemical analysis at neutral pH.

At pH 8, the CVs show only capacitive currents for all the studied materials (Fig. 6d). The magnitude of the currents follow the same trend as at pH 6 showing the highest current for the PANI-graphite composite and the lowest current for PANI. In the absence of electroactive species at $\text{pH}>8$, we can assume that the currents in the CVs are purely capacitive making it possible to estimate the differential capacitance of PANI, PANI-graphene and PANI-graphite. The differential capacitance is connected to the electrical double layer formation which enables the estimation of the total surface areas of these materials. Therefore, CVs of the neat PANI, PANI-graphene and PANI-graphite films were measured with the scan rates of 10, 25, 50, 100 and 200 mV s^{-1} (not shown here) in the potential interval of -0.2 V - 0.7 V at pH 10 to exclude the faradaic current contributions from the CVs. The average of the absolute values of the cathodic and anodic gravimetric current densities at 0.2 V were then plotted vs. the scan rate. The slope of the linear fit of these data points gives the differential capacitance which was 0.028, 0.121 and $0.309 \text{ } \mu\text{F g}^{-1} \text{ cm}^{-2}$ for PANI, PANI-graphene and PANI-graphite, respectively. We can therefore conclude that the differential capacitances (*i.e.* double layer capacitance at 0.2 V) of the PANI-

graphene and PANI-graphite composite films are 4.3 and 11.0 times higher, respectively, compared to the neat PANI film. A double layer capacitance of 178.5 mF cm^{-2} has been previously reported for PANI films measured in 2 M HCl [61], while 0.1 M HCl decreased the capacitance to $600\text{-}750 \text{ }\mu\text{F cm}^{-1}$ [62]. The much higher reported values compared to our capacitances are due to the fact that in the ICPs, the electrical double layer is formed by the charge residing on the polymer backbone which is compensated with oppositely charged counterions. The electrical double layer of ICPs differs from the double layer formed on the metal surfaces since it depends on the oxidation state of the ICP (*i.e.* the applied potential). It has been previously shown that the electrical double layer of the ICPs is almost absent at low potentials resulting in discharging of the ICP surface [63]. It must be pointed out that the differential capacitance of ICPs depends also on the film thickness which makes it difficult to compare capacitance values given in different studies without knowing the film thickness, porosity and surface roughness. In contrast to most ICPs, the PANI backbone can be discharged by both reduction and deprotonation. Therefore the same effect of depletion of the double layer should be expected for PANI at high pH and give rather low values of the differential capacitance. The most likely reason for the improved double layer capacitance of PANI-graphene and PANI-graphite is the incorporation of the carbon materials in the ICP matrix. The PANI-graphite composite material having the highest differential capacitance and reversibility of the reduction and oxidation reaction at $\text{pH} \geq 3$ is therefore the most promising composite material for electrochemical applications operating at neutral or slightly alkaline pH.

It has been recently shown that composite materials of PANI and GO, and rGO doped with Prussian Blue nanoparticles showed electrocatalytic effects towards the oxidation of ascorbic acid (AA), dopamine, uric acid [43] and hydrogen peroxide [64]. We have therefore used sodium ascorbate as a model substance to study its electrochemical oxidation on the neat PANI and PANI-graphite composite film surfaces in aqueous solutions of 10^{-4} - 10^{-2} M sodium ascorbate with 0.1 M KNO_3 functioning as

the supporting electrolyte (Fig. 7).

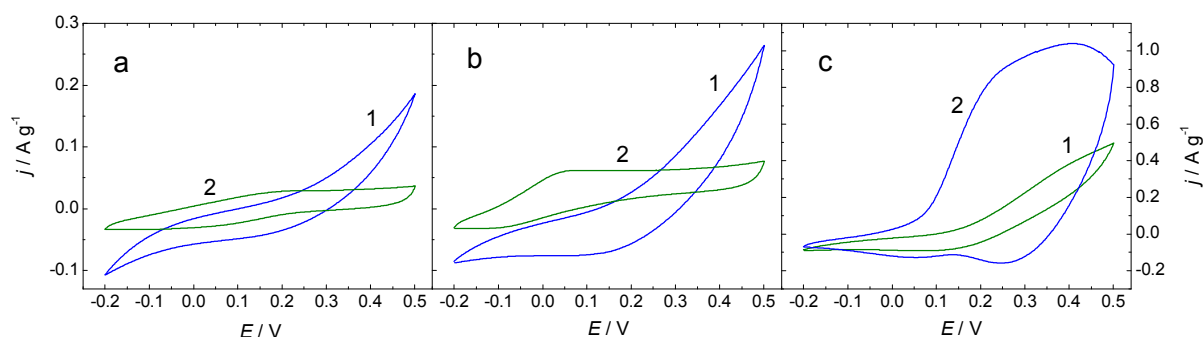


Fig. 7. Cyclic voltammograms of (1) neat PANI and (2) PANI-graphite films measured in (a) 0.1 M KNO_3 (background electrolyte, pH=6.5) and (b) 10^{-3} M and (c) 10^{-2} M sodium ascorbate (pH=7.3) solutions containing 0.1 M KNO_3 as the supporting electrolyte. The y-axis of (a) and (b) has the same scale. Reference electrode: Ag/AgCl/3 M KCl; $v=50 \text{ mV s}^{-1}$.

It is well known that ICPs and PANI in particular show electrocatalytic activity for the oxidation of AA at concentration $> 10^{-3}$ M (see Scheme 1 in [65]) giving rise to a new oxidation peak in the CV attributed to the AA oxidation [65]. This peak increases with the AA concentration and has its origin in the oxidation mechanism of AA in neutral or alkaline media [66], which is also valid for ascorbate anions. At neutral pH, ascorbate undergo an irreversible oxidation on the PANI surface resulting in the formation of free radicals which react further with the ascorbate anions to dehydroascorbic acid. This oxidation reaction results in release of protons and reduction of PANI. However, at moderate anodic potentials PANI is re-oxidized to the conducting form which is facilitated by the increased proton content (lower pH) at the film surface giving rise to the electrocatalytic effect. As it is shown in Fig. 7a, the electrochemical activity of neat PANI and PANI-graphite is rather low in the supporting electrolyte of 0.1 M KNO_3 in which the PANI-graphite film has oxidation and reduction peaks at *ca.* 0.18 and 0.04 V, respec-

tively. However, a new oxidation peak at *ca.* 0.05 V appears in the CV of PANI-graphite when 10^{-3} M sodium ascorbate was added to the supporting electrolyte (Fig. 7b; 10^{-4} M sodium ascorbate is shown in Fig. 8). This peak is not observed in the CV of neat PANI indicating that the electrocatalytic effect is more pronounced for the PANI-graphite composite film. Fig. 7c reveals that it becomes even more noticeable in the 10^{-2} M sodium ascorbate and shows a considerable difference in the gravimetric current densities compared to the neat PANI film. The electrocatalytic effect of PANI-graphite lowers also the offset potential for the increase of the oxidation current with *ca.* 0.1 V compared to neat PANI (Fig. 7c, curve 1) and the bare GC substrate (10^{-2} M AA in Fig. S4).

The electrocatalytic effect upon the oxidation of ascorbate at 0.2 V with the PANI and PANI-graphite electrodes are compared in Fig. 8. It is seen in the figure that the gravimetric current density for the oxidation of 10^{-4} M ascorbate is 1.3 times higher for PANI-graphite than for neat PANI. However, a signal amplification of 2.4 and 10.2 times were obtained by increasing the ascorbate concentration to 10^{-3} M and 10^{-2} M, respectively. As shown in Fig. 6, the PANI-graphite composite material is more electrochemically active at high pH compared to PANI. The measurements with ascorbic acid confirm this behaviour indicating that the PANI-graphite can be protonated easier than PANI at neutral pH. The reason for this is most likely the interaction of the conjugated structure of PANI with the sp^2 carbon atoms of graphite although the exact nature of the interaction is not known.

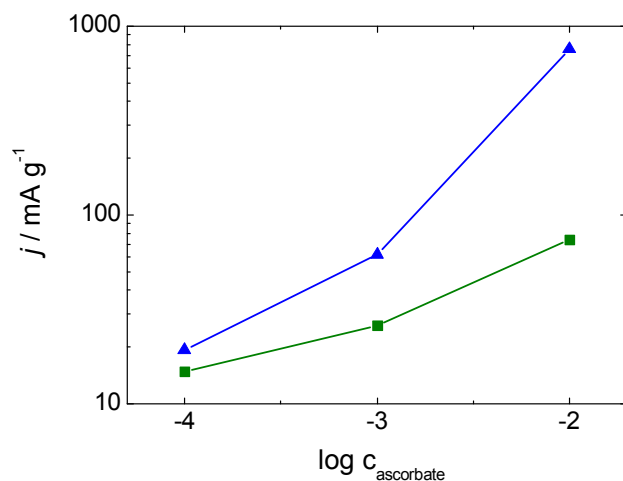


Figure 8. The current densities of (■) neat PANI and (▲) PANI-graphite films measured at 0.2 V in 10^{-4} - 10^{-2} M sodium ascorbate solutions containing 0.1 M KNO_3 as the supporting electrolyte.

4. Conclusions

We have shown that both few-layered graphene and exfoliated graphite form composite materials with PANI which can be dispersed in NMP. Cyclic voltammetric measurements conducted in the presence of the $\text{Ru}(\text{NH}_3)_6^{2+/3+}$ and $\text{Fe}(\text{CN})_6^{3-/4-}$ redox couples revealed that the exfoliated graphene/graphite forms a continuous network in the PANI matrix. This improved the electrochemical activity of the composite materials at $\text{pH} \leq 8$ and the pH stability of the conducting form of PANI. Due to the dispersibility of the PANI-graphene/graphite composites, thin films can be easily prepared and used for solid-state chemical sensor applications and as ion-to-electron transducers in solid-state ion-selective electrodes operating at the neutral and slightly alkaline pH, where the neat PANI is usually electrically non-conducting. We have used sodium ascorbate as a model substance to show the usefulness of the composite materials in chemical sensing applications. In comparison to neat PANI, a signal amplification of

10.2 times was obtained in the amperometric detection of 10^{-2} M ascorbate with the PANI-graphite film at pH 7.3 together with a subsequent lowering of the oxidation potential with ca. 0.1 V, demonstrating the electrocatalytic effect of the composite material. We are currently studying the application of the PANI-graphene/graphite composite materials as ion-to-electron transducers in solid-state ion-selective electrodes for ultratrace analysis.

Acknowledgments

Z.A.B. and T.L. gratefully acknowledge the Academy of Finland for financial support (project nos. 130588, 263656 and 257918). K.A.M. also thank the Centre for International Mobility (CIMO, Finland) for the research grant. Z.A.B. and K.A.M. are also grateful for funding from the Russian Foundation for Basic Research (RFBR) (project no. 14-03-31332).

References

- [1] A. K. Geim and K. S. Novoselov, *Nat. Mater.*, 2007, **6**, 183.
- [2] J. S. Bunch, A. M. van der Zande, S. S. Verbridge, I. W. Frank, D. M. Tanenbaum, J. M. Parpia, H. G. Craighead and P. L. McEuen, *Science*, 2007, **315**, 490.
- [3] Y. Xu, Y. Wang, J. Liang, Y. Huang, Y. Ma, X. Wan and Y. Chen, *Nano. Res.*, 2009, **2**, 343.
- [4] Y. Fan, J.-H. Liu, C.-P. Yang, M. Yu and P. Liu, *Sens. Actuators B, Chem.*, 2011, **157**, 669.
- [5] S. Liu, X. Xing, J. Yu, W. Lian, J. Li, M. Cui and J. Huang, *Biosens. Bioelectron.*, 2012, **36**, 186.
- [6] S. Park, Y. Shao, H. Wan, P. C. Rieke, V. V. Viswanathan, S. A. Towne, L. V. Saraf, J. Liu, Y. Lin and Y. Wang, *Electrochem. Commun.*, 2011, **13**, 258.
- [7] D. Wang, D. Choi, J. Li, Z. Yang, Z. Nie, R. Kou, D. Hu, C. Wang, L. V. Saraf, J. Zhang, I. A. Aksay and J. Liu, *ACS Nano*, 2009, **3**, 907.

- [8] J. Radich, P. McGinn and P. Kamat, *Electrochem. Soc. Interface*, 2011, **20**, 63.
- [9] S. Morales-Torres, L. M. Pastrana-Martínez, J. L. Figueiredo, J. L. Faria and A. M. T. Silva, *Environ. Sci. Pollut. Res. Int.*, 2012, **19**, 3676.
- [10] V. Tozzini and V. Pellegrini, *Phys. Chem. Chem. Phys.*, 2013, **15**, 80.
- [11] Z. A. Boeva and V. G. Sergeyev, *Polymer Sci. C*, 2014, **56**, 145.
- [12] L. Bay, K. West, B. Wintherjensen and T. Jacobsen, *Sol. Energy Mater. Sol. Cells*, 2006, **90**, 341.
- [13] J. Jang, *Adv. Poly. Sci.*, 2006, **199**, 189.
- [14] C. Barbero, H. J. Salavagione, D. F. Acevedo, D. E. Grumelli, F. Garay, G. A. Planes, G. M. Morales and M. C. Miras, *Electrochim. Acta*, 2004, **49**, 3671.
- [15] M. Baibarac and P. Gómez-Romero, *J. Nanosci. Nanotechnol.*, 2006, **6**, 289.
- [16] L. Dai L, *Aust. J. Chem.*, 2007, **60**, 472.
- [17] Y. Yang, C. Wang, B. Yue, S. Gambhir, C. O. Too and G. G. Wallace, *Adv. Energy Mater.*, 2012, **2**, 266.
- [18] K. Zhang, L. L. Zhang, X. S. Zhao and J. Wu, *Chem. Mater.*, 2010, **22**, 1392.
- [19] G. Wang, S. Zhuo and W. Xing, *Mater. Lett.*, 2012, **69**, 27.
- [20] A. V. Murugan, T. Muraliganth and A. Manthiram, *Chem. Mater.*, 2009, **21**, 5004.
- [21] H. Wang, Q. Hao, X. Yang, L. Lu and X. Wang, *Nanoscale*, 2010, **2**, 2164.
- [22] S. Ameen, M. S. Akhtar and H. S. Shin, *Sens. Actuators B, Chem.*, 2012, **173**, 177.
- [23] H. Bai, K. Sheng, P. Zhang, C. Li and G. Shi, *J. Mater. Chem.*, 2011, **21**, 18653.
- [24] A. Österholm, T. Lindfors, J. Kauppila, P. Damlin and C. Kvarnström, *Electrochim. Acta*, 2012, **83**, 463.

- [25] C. Mattevi, G. Eda, S. Agnoli, S. Miller, K. A. Mkhoyan, O. Celik O, D. Mastrogiovanni, G. Granozzi, E. Garfunkel and M. Chhowalla, *Adv. Funct. Mater.*, 2009, **19**, 2577.
- [26] S. Stankovich, R. D. Piner, X. Chen, N. Wu, S. T. Nguyen and R. S. Ruoff, *J. Mater. Chem.*, 2006, **16**, 155.
- [27] H.-J. Shin, K. K. Kim, A. Benayad, S.-M. Yoon, H. K. Park, I.-S. Jung, M. H. Jin, H.-K. Jeong, J. M. Kim, J.-Y. Choi and Y. H. Lee, *Adv. Funct. Mater.*, 2009, **19**, 1987.
- [28] J. Zhang, H. Yang, G. Shen, P. Cheng, J. Zhang and S. Guo, *Chem. Commun.*, 2010, **46**, 1112.
- [29] A. Viinikanoja, Z. Wang, J. Kauppila and C. Kvarnström, *Phys. Chem. Chem. Phys.*, 2012, **14**, 14003.
- [30] T. Lindfors, A. Österholm, J. Kauppila and M. Pesonen, *Electrochim. Acta*, 2013, **110**, 428.
- [31] T. Lindfors and R.-M. Latonen, *Carbon*, 2014, **69**, 122.
- [32] J. Yan, T. Wei, B. Shao, Z. Fan, W. Qian, M. Zhang and F. Wei, *Carbon*, 2010, **48**, 487.
- [33] H. Bai, Y. Xu, L. Zhao, C. Li and G. Shi, *Chem. Commun.*, 2009, 1667.
- [34] H. Gómez, M. K. Ram, F. Alvi, P. Villalba, E. Stefanakos and A. Kumar, *J. Power Sources*, 2011, **196**, 4102.
- [35] T. Lindfors and L. Harju, *Synth. Met.*, 2008, **158**, 233.
- [36] E. Coskun, E. A. Zaragoza-Contreras and H. J. Salavagione, *Carbon*, 2012, **50**, 2235.
- [37] J. Luo, S. Jiang, R. Liu, Y. Zhang and X. Liu, *Electrochim. Acta*, 2013, **96**, 103.
- [38] J. Luo, Y. Chen, Q. Ma, R. Liu and X. Liu, *RSC Adv.*, 2013, **3**, 17866.
- [39] L. Al-Mashat, K. Shin, K. Kalantar-Zadeh, J. D. Plessis, S. H. Han, R. W. Kojima, R. B. Kaner, D. Li, X. Gou, S. J. Ippolito and W. Wlodarski, *J. Phys. Chem. C*, 2010, **114**, 16168.

- [40] X. Huang, N. Hu, R. Gao, Y. Yu, Y. Wang, Z. Yang, E. S.-W. Kong, H. Wei and Y. Zhang, *J. Mater. Chem.*, 2012, **22**, 22488.
- [41] M. Parmar, C. Balamurugan and D.-W. Lee, *Sensors*, 2013, **13**, 16611.
- [42] K. Chen, Z.-L. Zhang, Y.-M. Liang and W. Liu, *Sensors*, 2013, **13**, 6204.
- [43] P. Manivel, M. Dhakshnamoorthy, A. Balamurugan, N. Ponpandian, D. Mangalaraj and C. Viswanathan, *RSC Adv.*, 2013, **3**, 14428.
- [44] K. R. Paton, E. Varrla, C. Backes, R. J. Smith, U. Khan, A. O'Neill, C. Boland, M. Lotya, O. M. Istrate, P. King, T. Higgins, S. Barwich, P. May, P. Puczkarski, I. Ahmed, M. Moebius, H. Pettersson, E. Long, J. Coelho, S. E. O'Brien, E. K. McGuire, B. M. Sanchez, G. S. Duesberg, N. McEvoy, T. Pennycook, C. Downing, A. Crossley, V. Nicolosi and J. N. Coleman, *Nat. Mater.*, 2014, **13**, 624.
- [45] J. Bobacka, A. Ivaska and A. Lewenstam, *Chem. Rev.*, 2008, **108**, 329.
- [46] T. Lindfors, L. Höfler, G. Jágerszki and R. E. Gyurcsányi, *Anal. Chem.*, 2011, **83**, 4902.
- [47] F. M. Smits, *Bell. Syst. Tech. J.*, 1958, **37**, 711.
- [48] The NIST X-ray Photoelectron Spectroscopy (XPS) Database,
http://srdata.nist.gov/xps/intro.aspx_n.d.
- [49] K. Zhang, Y. Zhang and S. Wang, *Sci. Rep.*, 2013, **3**, 3448.
- [50] T. Szabó, O. Berkesi, P. Forgó, K. Josepovits, Y. Sanakis, D. Petridis and I. Dékány, *Chem. Mater.*, 2006, **18**, 2740.
- [51] Y. Wu, B. Wang, Y. Ma, Y. Huang, N. Li, F. Zhang and Y. Chen, *Nano Res.*, 2010, **3**, 661.
- [52] C. Laslau, Z. D. Zujovic, L. Zhang, G. A. Bowmaker and J. Travas-Sejdic, *Chem. Mater.*, 2009, **21**, 954.
- [53] J. Tang, X. Jing, B. Wang and F. Wang, *Synth. Met.*, 1988, **24**, 231.

- [54] M. Trchova, J. Stejskal and J. Prokeš, *Synth. Met.*, 1999, **101**, 840.
- [55] S. Liu, J. Tian, L. Wang, Y. Luo and X. Sun, *Analyst*, 2011, **136**, 4898.
- [56] T. Lindfors, A. Österholm, J. Kauppila and R. E. Gyuresányi, *Carbon*, 2013, **63**, 588.
- [57] S. Stafström, B. Sjögren and J. L. Brédas, *Synth. Met.*, 1989, **29**, 219.
- [58] R. Sivakumar and R. Saraswathi, *Synth. Met.*, 2003, **138**, 381.
- [59] D. Stilwell and S. Park, *J. Electrochem. Soc.*, 1989, **136**, 427.
- [60] T. Lindfors, H. Sandberg and A. Ivaska, *Synth. Met.*, 2004, **142**, 231.
- [61] S. Leinad Gnana Lissy, S. Pitchumani and K. Jayakumar, *Mater. Chem. Phys.*, 2002, **76**, 143.
- [62] E. Kazimierska, M. R. Smyth, and A. J. Killard, *Electrochim. Acta*, 2009, **54**, 7260.
- [63] J. Wang and A. J. Bard, *J. Am. Chem. Soc.*, 2001, **123**, 498.
- [64] N. Zhu, S. Han, S. Gan, J. Ulstrup and Q. Chi, *Adv. Funct. Mater.*, 2013, **23**, 5297.
- [65] A. Ambrosi, A. Morrin, M. R. Smyth and A. J. Killard, *Anal. Chim. Acta*, 2008, **609**, 37.
- [66] R. P. Kalakodimi and M. Nookala, *Anal. Chem.*, 2002, **74**, 5531.